

# Wearable inertial sensors for arm motion tracking in home-based rehabilitation

Huiyu Zhou<sup>a,1</sup>, Huosheng Hu<sup>a</sup> and Nigel Harris<sup>b</sup>

<sup>a</sup> *University of Essex, Colchester, CO4 3SQ, UK*

<sup>b</sup> *University of Bath, Bath, BA1 1RL, UK*

**Abstract.** We in this paper introduce a real-time human arm movement tracking system that can be used to aid the rehabilitation of stroke patients. A 3-axis inertial sensor is used to capture arm movements in 3-D space and in real time. The tracking algorithm is based on a kinematical model that just considers the human forearms at this stage. To improve accuracy and consistency, a Lagrangian based filtering strategy is adopted. The experimental results demonstrate that the proposed framework can be used to track forearm motion.

**Keywords.** Rehabilitation, motion tracking, inertial sensor, filtering

## 1. Introduction

Stroke is the biggest cause of severe disability in the UK. Ten thousand people each year experience a first stroke, and a further 30,000 have a further stroke [5]. More than 75% of these people require multi-disciplinary assessments and appropriate rehabilitative treatments after they are discharged from hospital [1]. This places a large demand on community healthcare services, which often have quite limited therapy resources. As a result, there is considerable interest in training aids or intelligent systems that conduct rehabilitation in patient's home environment rather than in hospital.

The goal of rehabilitation is to enable a person who has experienced a stroke to regain the highest possible level of function. Although some functional abilities may be spontaneously restored soon after a stroke, recovery is an ongoing process and the patient must perform repeatative movements, correcting any undesired motion behavior in order to regain fine control of the upper or lower limbs. During these rehabilitation exercises, if the movements of stroke patients can be tracked incorrect motion patterns can be readily identified and corrected. Therefore, devices that can accurately track the position of limbs in space is an essential component of such a rehabilitation system. Here, we will briefly summarize the existing human tracking systems, which can be classified as non-vision based, vision-based with markers, vision-based without markers, and robot-guided systems.

*Non-vision based:* Systems can deploy sensors, e.g. inertial, mechanical and magnetic ones, to continuously collect movement information. For example, inertial and

---

<sup>1</sup>Correspondence to: H. Zhou, Department of Computer Science, University of Essex, Colchester, UK. Tel.: +44 1206 874092; Fax: +44 1206 872788; E-mail: zhou@essex.ac.uk.

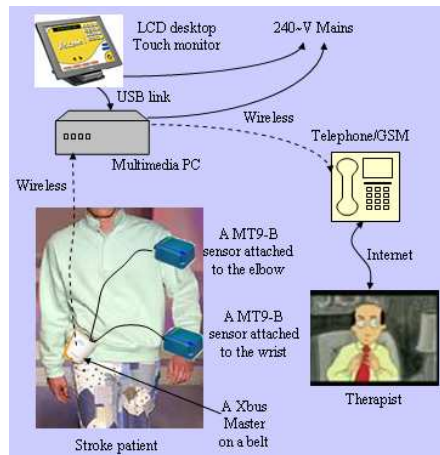


**Figure 1.** Illustration of the proposed rehabilitation system.

magnetic sensors based devices (i.e. [6]) exploit micro-electromechanical systems (MEMS). These devices can be used in most circumstances without any limitations (i.e. illumination, temperature, or space, etc.). They have better performance in accuracy against mechanical sensors based devices. The main drawback of using inertial sensors is that accumulating errors (or drift) will become significant after a short period of time.

*Vision-based with markers:* Numerous marker-based tracking systems are nowadays available in markets and academics. CODA (Charnwood Dynamics, UK) and Qualisys (Qualisys AB, Sweden) are two examples: the former uses “active” markers, and the latter exploits “passive” markers that are grasped by the allocated cameras. However, these systems inevitably suffer from the occlusion problem due to the existence of the line of sight.

*Vision-based without markers:* As a less restrictive motion capture technique, markerless based sensing is capable of partially overcoming the occlusion problem as it concerns boundaries or features on human bodies. This approach has a robust performance but is inefficient in computation and less effective in rigorous circumstances. To solve the inefficiency problem, for example, Mihailidis *et al.* [3] designed a sensing agent for an intelligent environment that assists older people with dementia during their life. It has shown promising results of 2-D hand motion tracking. However, this system failed to provide 3-D motion estimation.

*Robot-guided:* To find out whether exercise therapy influences plasticity and recovery of the brain following a stroke, an automatic system, named MIT-MANUS, was designed to move, guide, or perturb the movement of a patient’s upper limb, whilst recording motion-related quantities, e.g. position, velocity, or forces applied [2]. This system was successfully implemented. Unfortunately, during exercise then arms has to be attached to the robot arm so the patient is unable to carry out free motion.

In this paper, a kinematic model of human forearm motion is developed, which can provide consistent estimates of forearm movements such as position and orientation based on a commercially available inertial sensor MT9 (Xsens Motion Technology, Holland). At this preliminary stage, the tracking system requires the elbow joint to be fixed,

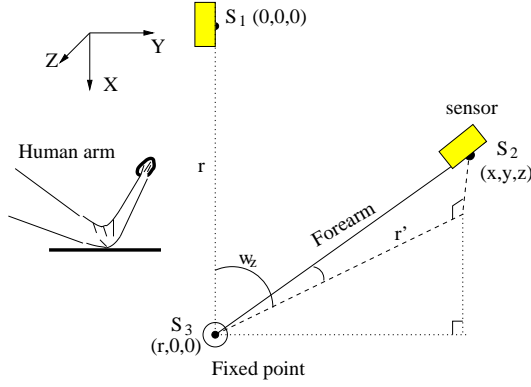


**Figure 2.** Kinematics of a human forearm (the fixed point is the elbow joint).

however later work will remove this constraint. The designed motion tracking framework has been integrated within a home-based rehabilitation system illustrated in Figure 1.

The rest of the paper is organized as follows. Section 2 presents a novel approach to conduct the 3-D tracking based on the collected angular rate, which exploits the kinematics of the human forearm movements. A weighted least squares filtering method is proposed in Section 3 that reduces the errors whose Euclidean distance is larger than a threshold. Section 4 introduces experimental results. Conclusions and future work are finally provided in Section 5.

## 2. Kinematic modelling of human arm motion

A kinematic model of the forearm is proposed in this section. Consider a rigid human forearm moving in the 3-D inertial space. Figure 2 shows the kinematics of a human forearm, where the elbow presumably is fixed and the inertial sensor is attached nearby the wrist.  $r$  is the distance between the the centre of the sensor and the fixed point, which can be known *a priori*.

Let the coordinates of an arbitrary point be denoted by  $u(x, y, z)$ , then one can have projected coordinates on three orthogonal planes, i.e.  $x$ - $y$  plane

$$\begin{cases} x = r - \sqrt{r^2 - z^2} \cos \omega_z \\ y = \sqrt{r^2 - z^2} \sin \omega_z \end{cases} \quad (1)$$

$y$ - $z$  plane

$$\begin{cases} y = \sqrt{r^2 - x^2} \cos \omega_x \\ z = \sqrt{r^2 - x^2} \sin \omega_x \end{cases} \quad (2)$$

$x$ - $z$  plane

$$\begin{cases} x = r - \sqrt{r^2 - y^2} \sin \omega_y \\ z = \sqrt{r^2 - y^2} \cos \omega_y \end{cases} \quad (3)$$

where  $\omega_x$ ,  $\omega_y$  and  $\omega_z$  are Euler angles around  $x$ -,  $y$ - and  $z$ -axis, respectively.

Assume that  $a = (\cos \omega_x)^2$ ,  $b = (\cos \omega_y)^2$  and  $c = (\cos \omega_z)^2$ .  $x$  then is

$$x = \frac{r \pm r \sqrt{1 - (1 + abc)(1 - c + bc - abc)}}{1 + abc} \quad (4)$$

Substituting Equation (4) to the remainders of Equation (1), (2) and (3), the solutions for  $y$  and  $z$  will be explicitly available as follows

$$\begin{cases} y = \sqrt{r^2 - z^2} \sin \omega_z \\ z = \sqrt{r^2 - x^2} \sin \omega_x \end{cases} \quad (5)$$

Solutions for  $x$ ,  $y$  and  $z$  rely on the estimated Euler angles, which are the integration of the collected turning-rates [7]. The angles usually accompany noise or drifts due to the inertial properties. These errors might be up to  $5^\circ$  or more, which can significantly bias the estimated 3-D positions. One example is shown in Figure 3, where one can see significant discrepancy between the estimates of  $x$ -axis position by a standard motion tracker and our method, respectively. So, a real-time filter is needed for restoring the true data.

### 3. Real time filtering

We intend to reconstruct a true data point  $u$  from its observation  $\tilde{u}$  (e.g.  $x$ ,  $y$  and  $z$  positions)

$$\tilde{u} = u + \epsilon \quad (6)$$

where  $\epsilon$  is noise or an unknown error. One of the common denoising techniques is to minimise a function of gradient given as

$$\min_u F_{\epsilon,p}(u), \text{ and, } F_{\epsilon,p}(u) = \int_{\Omega} |\nabla^\epsilon u|^p dx + \lambda \|\tilde{u} - u\|^2, \quad (7)$$

where  $\lambda \geq 0$  is a Lagrange multiplier, and  $\epsilon$  is a regularization coefficient:

$$|\nabla^\epsilon u| = (u^2 + \epsilon^2)^{\frac{1}{2}}. \quad (8)$$

To solve the minimisation problem, Equation (7), we use the *Euler-Lagrange equation* as follows:

$$u_1 = \nabla \cdot \left( \frac{\nabla u}{|\nabla^\epsilon u|^{2-p}} \right) + \beta(\tilde{u} - u), \quad (9)$$

where  $\beta (= \frac{2\lambda}{p})$  is the *constraint parameter* (indicating the descent direction), and  $\lambda$  can be available if we take the derivative for Equation (7) with respect to  $u$  and then set it to zero. The required derivatives are yielded as follows:

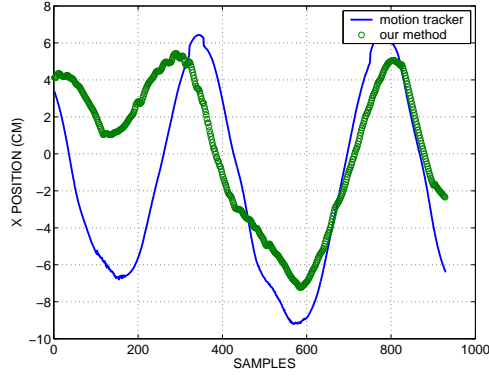


Figure 3. Discrepancy between the estimates by a standard motion tracker and our method, respectively.

$$\begin{aligned}
 \frac{\partial x}{\partial \omega_x} &= \frac{2rab^2c^2 \sin \omega_x}{(1+a^2b^2c^2)^2} - \frac{2rab^2c^2d \sin \omega_x}{(1+a^2b^2c^2)^2} + \frac{rab^2c^2 \sin \omega_x (-c^2+b^2c^2-2a^2b^2c^2)}{(1+a^2b^2c^2)d}; \\
 \frac{\partial x}{\partial \omega_y} &= \frac{2ra^2bc^2 \sin \omega_y}{(1+a^2b^2c^2)^2} - \frac{2ra^2bc^2d \sin \omega_y}{(1+a^2b^2c^2)^2} + \frac{ra^2bc^2 \sin \omega_y (1-c^2+b^2c^2-a^2b^2c^2)}{(1+a^2b^2c^2)d} + \\
 &\quad r(-bc^2 \sin \omega_y + a^2bc^2 \sin \omega_y); \\
 \frac{\partial x}{\partial \omega_z} &= \frac{2ra^2b^2c \sin \omega_z}{(1+a^2b^2c^2)^2} - \frac{2ra^2b^2cd \sin \omega_z}{(1+a^2b^2c^2)^2} + \frac{ra^2b^2c \sin \omega_z (1-c^2+b^2c^2-a^2b^2c^2)}{(1+a^2b^2c^2)d} + \\
 &\quad r(c \sin \omega_z - b^2c \sin \omega_z + a^2b^2c \sin \omega_z); \\
 \frac{\partial z}{\partial \omega_x} &= -\frac{x \frac{\partial x}{\partial \omega_x} \sin \omega_x}{\sqrt{r^2-x^2}} + \sqrt{r^2-x^2}a; \quad \frac{\partial z}{\partial \omega_y} = -\frac{x \frac{\partial x}{\partial \omega_y} \sin \omega_x}{\sqrt{r^2-x^2}}; \\
 \frac{\partial z}{\partial \omega_z} &= -\frac{x \frac{\partial x}{\partial \omega_z} \sin \omega_x}{\sqrt{r^2-x^2}}; \quad \frac{\partial y}{\partial \omega_x} = -\frac{z \frac{\partial z}{\partial \omega_x} \sin \omega_z}{\sqrt{r^2-z^2}}; \\
 \frac{\partial y}{\partial \omega_y} &= -\frac{z \frac{\partial z}{\partial \omega_y} \sin \omega_z}{\sqrt{r^2-z^2}}; \quad \frac{\partial y}{\partial \omega_z} = -\frac{z \frac{\partial z}{\partial \omega_z} \sin \omega_z}{\sqrt{r^2-z^2}} + \sqrt{r^2-z^2}c.
 \end{aligned} \tag{10}$$

where  $d = \sqrt{1 - (1 + a^2b^2c^2)(1 - c^2 + b^2c^2 - a^2b^2c)}$ . When  $p = 1$  and  $\varepsilon = 0$ , Equation (7) will become a problem of *total variation* (TV) [4].

However, noise or outliers often exist in the estimation because of irregular motion or the soft-skin effect, etc. These points possibly mislead the solution by Equation (7) to an incorrect position. To remove these errors before computing, we explore a smoothing scheme: in a small neighborhood, the point with the variance of the Euclidean distance between its position and the weight centre of the region larger than twice of the averaging variance will be considered as errors and be removed from the computation list. From the efficient point of view, the size of the neighborhood is 5-7. This filtering strategy is illustrated in Figure 4, where square 7 is the filtered output of circle 7 given the previous seven points, and the dotted circle consists of the inliers.

To conduct a fast minimization for Equation (8), we use the iterative Levenberg-Marquardt (L-M) algorithm. Although L-M can only seek a locally optimal solution, we wish that it converges to the correct solution by setting the starting point as the weight centre of the investigated point area.

#### 4. Experimental work

To evaluate the performance of the filter-on kinematic model against the filter-off technique, we make use of a commercial human motion tracking system ("Qualysis"). This

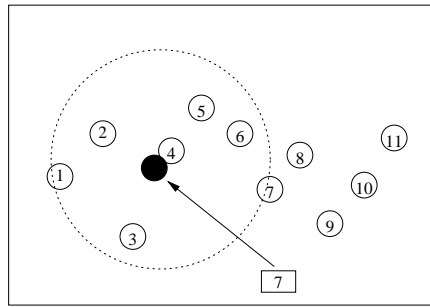


**Figure 4.** Illustration of the denoising strategy.

system provides absolute positions for the human arm movements during trajectories. Qualysis uses retro-reflective ball markers that can be identified by the cameras surrounding the object person. It directly reconstructs 3-D positions of the moving human limbs after proper calibration is achieved.

To set up the experimental environment, a Qualysis marker is attached to one side of the wrist joint while the MT9 inertial sensor is mounted on the other side. This method has better accuracy than the configuration where the marker and the inertial sensor both are placed on the same side. The distance between the elbow joint (fixed point) and the centre of the sensor is 24 cm. Figure 5 illustrates the experimental set-up in which the “Qualysis” has 3 video cameras to observe upper limb movements via the ball marker. Before the experiments start, we need to run a calibration for aligning the coordinate system of the inertial sensor with that of the Qualysis system.

Inertial measurements can be obtained by going through the following procedure. The MT9 inertial sensor collects data and then pre-filters it to remove high-frequency noise. This is followed by computing the 3-D position and orientation based on the proposed kinematical modelling. Due to the presence of noise and errors a dynamic filter is applied for suppressing the noise or errors. This process will run continuously until it is manually terminated. In the experiments, these two systems work independently and asynchronously, so we cannot directly compare their 3-D motion estimations. A simple way to get around this problem is to develop a “least-squared fitting” method, which is used to fit individual estimates to one-cycle curves (see Figures 6 and 7). By doing this, one can easily judge whose performance is better.

A number of repeated motion patterns have been captured in order to obtain comprehensive comparisons. In this paper, only two cases are investigated: (1) up-down motion, and (2) cyclic rotation in 3-D space. It should be noticed that the elbow joint is kept stationary on the testing bench during the forearm movements.

#### *Case 1: up-down movements*

In this experiment, the up-down forearm motion is captured by both the MT9 inertial sensor and the “Qualysis” tracking system. Figure 6 shows 3-D motion trajectories of the forearm movements that are captured. Note, the solid line is the “Qualysis” data, the dashed line is the inertial data after filtering, and the dotted line is the inertial data without filtering. These results are the mean values produced by the weighted least-square calculation. The mean error between the “Qualysis” data and the inertial data after filter-

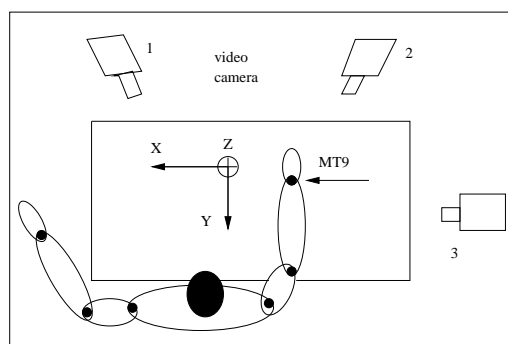


**Figure 5.** Illustration of the experimental set-up.

ing is 1.09 cm (SD: 0.47 cm), while the mean error between the “Qualysis” data and the inertial data without filtering is 1.52 cm (SD: 1.05 cm).

#### *Case 2: cyclic rotation*

Figure 7 shows 3-D motion trajectories of this motion style, and the symbols can be referred to the earlier description. The mean error between the “Qualysis” data and the inertial data after filtering is 1.73 cm (SD: 0.93 cm), while the mean error between the “Qualysis” data and the inertial data without filtering is 2.27 cm (SD: 1.56 cm).

## 5. Conclusions and future work

We have presented a wearable inertial sensing based tracking system that integrates kinematics of human arm movements and a dynamic filtering strategy. Compared to the commercial tracking system “Qualysis” that uses markers, our system is able to deliver real time human forearm motion estimation with a simple set-up. Also, our system has achieved reasonably accurate results. The future work will be addressed to extend the ideas presented here in order to implement a portable device that considers real three-joints arm movements with higher degrees of freedom. The kinematic model of the upper arm is the same as that of the forearm, although the fixed point is now located at the shoulder. Another MT9 sensor will be used to represent this motion.

## Acknowledgements

This is part of SMART Rehabilitation Project funded by the UK EPSRC under Grant GR/S29089/01. We are grateful to Ms Yaqin Tao for helping us to set up the experiments.

## References

- [1] J.H. Cauraugh, S. Kim, *Two coupled motor recovery protocols are better than one electromyogram-triggered neuromuscular stimulation and bilateral movements*, *Stroke* **33** (2002), 1589–1594.

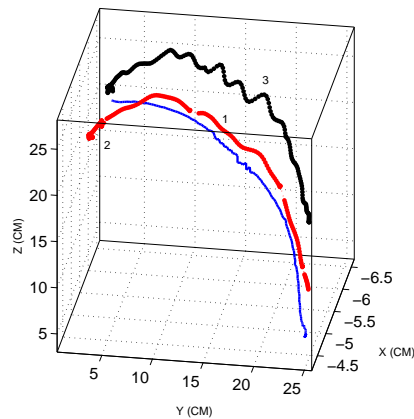


**Figure 6.** Case 1 - Up-down motion trajectories: the "Qualysis" data (solid line - 1), the inertial data after filtering (dashed line - 2) and the inertial data without filtering (dotted line - 3).

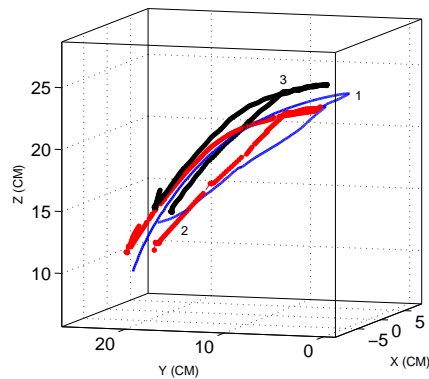


**Figure 7.** Case 2 - Cyclic motion trajectories: the "Qualysis" data (solid line - 1), the inertial data after filtering (dashed line - 2) and the inertial data without filtering (dotted line - 3).

- [2] H.I. Krebs, B.T. Volpe, M.L. Aisen, N. Hogan, *Increasing productivity and quality of care: robot-aided neuro-rehabilitation*, Journal of rehabilitation research and development **37** (2000), 639–652.
- [3] A. Mihailidis, B. Carmichael, J. Boger, *The use of computer vision in an intelligent environment to support aging-in-place, safety, and independence in the home*, IEEE Transaction on information technology in medicine **8** (2004), 238–247.
- [4] L. Rudin, S. Osher, E. Fatemi, *Nonlinear total variation based noise removal algorithms*, Physica **60** (1992), 259–268.
- [5] The Stroke Association, *Speaking out about stroke services*, London: the Stroke Association, 2001.
- [6] H. Zheng, N.D. Black, and N.D. Harris, *Position-sensing technologies for movement analysis in stroke rehabilitation*, Medical & Biological Engineering & Computing **43** (2005), 413–420.
- [7] H. Zhou, H. Hu, *Inertial motion tracking of human arm movements in home-based rehabilitation*, Proc. of IEEE Int. Conf. on Mechatronics and Automation, Niagara Falls, Canada, 2005.